EXTREME WAVE LOAD SIMULATIONS ON AN OSCILLATING WATER COLUMN WAVE ENERGY CONVERTER

Nhu Nguyen, Chris Chartrand, Borja de Miguel Para, Jon Morgaetxebarria Aurrekoetxea

Abstract— **Extreme load analysis is an essential step in the design of structural and mooring systems for wave energy converters (WEC). The current study aims to evaluate the structural loads on the MARMOK Oscillating Water Column (OWC) WEC under both regular and irregular wave conditions, as well as to evaluate the effectiveness of its station keeping (mooring) systems. The project employs the open-source computational fluid dynamics simulation software OpenFOAM to model the fully moored floating system. The WEC device hydrodynamics are validated against laboratory data for free decay in heave and pitch motions. In addition, the station keeping model is validated against mooring tension static offset tests and benchmarked against experimental data in irregular waves. An elegant method of numerically recreating irregular wave inflow conditions from empirical measurements is shown which allows for consistent comparison between the model and experimental results. The calibrated numerical model is then employed to study the full-scale system's responses. Preliminary results of structural loadings on the fixed and floating spar buoy (with one mooring configuration as sample) are presented in the paper.**

Keywords— **WEC, OWC, wave energy converter, MARMOK, OpenFOAM, CFD, irregular, extreme wave.**

I. INTRODUCTION

GIVEN the detrimental environmental issues like acid rain and global warming, the transition from conventional energy sources such as petroleum and coal becomes an imminent step. Alongside wind energy, wave energy converters (WECs) have long been recognized as a competitive option for harnessing and converting energy from surface waves into usable electricity [1]. The untapped wave energy potential worldwide is estimated to be around 30,000 trillion watt-hours per year [2], which has led to a significant increase in research interest in this field in recent years.

Despite extensive efforts, the development of wave energy extraction remains predominantly in the research and development (R&D) stage, with only a few systems installed in real offshore conditions [3]. Reducing the cost of wave energy converter technology, primarily driven by extreme wave loads, is identified as a crucial pathway for its advancement [4]. Therefore, it is essential to examine the impact of extreme events on WECs and ensure the survivability of WEC systems in offshore extreme conditions, as these factors significantly influence the cost of wave energy technology.

According to IEC TS 62600-2, the design of a wave energy converter should consider the sea states along the 50-year environmental contour that produces the largest response. However, reproducing these large waves in experimental wave tanks is challenging and expensive. Consequently, numerical tools play a fundamental role in understanding wave-structure interaction. While potential flow methods are commonly used for modelling wave-structure interaction with small-amplitude waves, they are not suitable for modelling extreme waves, which are characterized by high steepness, nonlinearity, and large structural responses. A study conducted on extreme loading in a two-body WEC using a combination of mid- and high-fidelity numerical modelling tools revealed that high-fidelity models are necessary to capture the upper bound of wave loads [5].

To address these effects, the most widely used high-fidelity approach based on computational fluid dynamics (CFD) is the incompressible two-phase Reynolds-averaged Navier-Stokes (RANS). Although CFD models are computationally more expensive than low- and mid-fidelity tools, they offer several advantages, including the ability to simulate nonlinear waves, account for viscous effects, model wave overtopping, and accurately evaluate the dynamics of WECs [6]. Moreover, CFD codes have the potential to complement or replace costly, and time-consuming experimental campaigns.

Nhu Nguyen is with Sandia National Laboratories, 1515 Eubank SE, Albuquerque, NM 87123, USA. (e-mail: nnguye@sandia.gov).

Chris Chartrand is with Sandia National Laboratories, 1515 Eubank SE, Albuquerque, NM 87123, USA. (e-mail: ccchart@sandia.gov).

Borja de Miguel Para is with IDOM Consulting, Engineering, Architecture S.A.U (e-mail: bdemiguel@idom.com).

Jon Morgaetxebarria Aurrekoetxea is with IDOM Consulting, Engineering, Architecture S.A.U

(e-mail: jmorgaetxebarria@idom.com).

Digital Object Identifier: https://doi.org/10.36688/ewtec-2023-291

Numerous studies in literature have focused on benchmarking the performance of CFD models. These studies compare the traditional mesh-based CFD performance with scaled tank testing, higher fidelity techniques such as meshless Smoothed Particle Hydrodynamics, or lower fidelity modelling approaches like potential flow. For example, mid- and high-fidelity numerical models have been successfully employed to assess the response of two taut-moored WEC-like buoys in focused waves [7]. Extensive validation was conducted using a CFD-based numerical wave tank for the 1:5, and 1:20 scale WaveStar point-absorber device in [8][9], and a CFD-based model was developed and validated for a fixed and freely-pitching 1:10 scale model of the WaveStar in [10].

Other studies have focused on the survivability of WECs in extreme wave conditions including the simulation of 100-year return period waves interacting with a WEC using RANS equations presented in [11]. The authors employed the numerical model to investigate the impact of alternating damping in the power-take-off system. Modelling interactions of 50-year return period waves on a point-absorber WEC using CFD was also employed to study the highly nonlinear effects like breaking waves and slamming loads in [12]. Two different CFD programs OpenFOAM (OF) and ANSYS Fluent along with a linear model were examined in modelling a point absorbing WEC in extreme waves. The study concluded that OpenFOAM can achieve higher accuracy than ANSYS Fluent, however it also demands higher computational resources. The linear model, on the other hand, is not sufficient for high and extreme wave cases [13]. It is, however, worth noting that the majority of CFD model validation studies for WEC systems have primarily focused on regular or extreme regular waves, leaving a limited number of studies on numerical simulations of WEC performance under extreme irregular waves.

To address this research gap and provide more insights into employing CFD for survival condition analysis, the present study aims to develop and validate a high-fidelity CFD model for a 1:28 scale oscillating water column (OWC) WEC MARMOK operating in extreme irregular wave conditions [14]. The numerical procedures employed closely follow those utilized in the corresponding experimental campaign, as reported in [14]. The extreme irregular wave inflow conditions, derived from empirical measurements, are accurately reproduced to facilitate consistent comparisons between the model and experimental results. Furthermore, the hydrodynamics of the WEC device are validated against laboratory data obtained from free decay tests involving heave and pitch motions. The study employs the overset approach to model the wave-structure interaction under extreme conditions, which often leads to significant system motion. The fluid and motion solvers utilize OpenFOAM package version v2106, while the dynamic mooring modelling toolbox MoorDyn [15] is employed to simulate the behavior of the mooring system. Wave generation and absorption are modelled using the wave2Foam toolbox [16].

The remaining sections of the paper are organized as follows: Section 2 provides an overview of the numerical modelling technique. Section 3 outlines experimental setup and the WEC system. Section 4 presents a comprehensive analysis of the numerical results, along with a thorough comparison against the experimental data. Finally, Section 5 summarizes the key findings and conclusions drawn from this study.

II. NUMERICAL MODELLING

A. Numerical method

The governing equations for the motion of an incompressible and isothermal Newtonian fluid based on the Reynolds-Averaged Navier-Stokes (RANS) approach, can be expressed through the conservation of mass (1) and momentum (2) as follows.

$$\frac{\partial \rho}{\partial t} + \nabla \cdot (\rho \boldsymbol{U}) = 0 \tag{1}$$

$$\frac{\partial \rho \boldsymbol{U}}{\partial t} + \nabla \cdot (\rho \boldsymbol{U}\boldsymbol{U}) = -\nabla p + \nabla \cdot \boldsymbol{S} + \rho \boldsymbol{f}_b \tag{2}$$

Where $\boldsymbol{U}$ and ρ represents the velocity vector, and the fluid density, respectively. $\boldsymbol{S}$ is the viscous stress tensor, and $\boldsymbol{f}_b$ denotes the external forces.

In the case of two-phase simulations, an additional equation is required to describe the motion of the phases. The volume of fluid method, as described in [17], is employed to capture the free water surface. The phase fraction, denoted by α, is utilized to represent the mixture between air (α = 0) and water (α = 1). The two-phase problem is treated as a single fluid, and the local properties including density and dynamic viscosity, μ are subsequently calculated as follows

$$\rho = \alpha \rho_{water} + (1 - \alpha)\rho_{air} \tag{3}$$

$$\mu = \alpha \mu_{water} + (1 - \alpha)\mu_{air} \tag{4}$$

The conservation of phase fraction is also enforced by employing

$$\frac{\partial \alpha}{\partial t} + \nabla \cdot (\boldsymbol{U}\alpha) + \nabla \cdot \left(\boldsymbol{U}_c \alpha (1 - \alpha)\right) = 0 \tag{5}$$

With

$$|U_c| = \min[c_\alpha |U|, \max(|U|)]$$

$\boldsymbol{U}_c$ represents the artificial compressive velocity factor $c_\alpha = 1$. To enforce the phase fraction to be within the range of [0, 1] and preserve sharp interfaces during the CFD simulation, the multi-dimensional limiter for explicit solutions (MULES) technique, as described in [18], is employed for the solutions.

When dealing with high and steep waves, significant responses in the WEC are expected, necessitating the adaptation of the computational mesh to accommodate these large deformations. OpenFOAM provides support for various dynamic mesh methods, enabling the computational mesh to evolve over time in accordance with the structure's motions resulting from wave interaction.

In recent versions of OpenFOAM (starting v1706), overset mesh functionality has been introduced alongside the existing morphing mesh. The overset mesh technique offers the capability to simulate complex geometries interacting with different wave conditions while maintaining a high-quality mesh around both the solid body geometry and around the wave surface [19].

The OpenFOAM sixDoFRigidBodyMotion library is employed to obtain the motion of the body in six degrees of freedom (DoF). This library utilizes Newton's second law to calculate the body's response, considering the forces and moments generated by the excitation of ocean waves and any additional external loads, such as mooring and/or the power take-off (PTO) forces.

B. Wave generation and absorption

This study utilizes the waves2Foam library, a comprehensive toolbox specifically designed for generating and absorbing free surface water waves using relaxation zones. These relaxation zones can be specified to either generate waves at the inlet and/or absorb waves (via passive approach [16]) at the outlet. Inside these relaxation zones, the computed solution for velocity and volume fraction (u_c, α_c) are blended with an analytical target solution (u_t, α_t) such as

$$u_c = u_c\varphi(\boldsymbol{x}) + u_t\big(1 - \varphi(\boldsymbol{x})\big) \tag{6}$$

$$\alpha_c = \alpha_c\varphi(\boldsymbol{x}) + \alpha_t\big(1 - \varphi(\boldsymbol{x})\big) \tag{7}$$

Where φ denotes the spatially varying weighting function with $\varphi(\boldsymbol{x}) \in [0,1]$; 0 is at the outer boundary and 1 is at the internal boundary of the relaxation zone (Fig. 1).

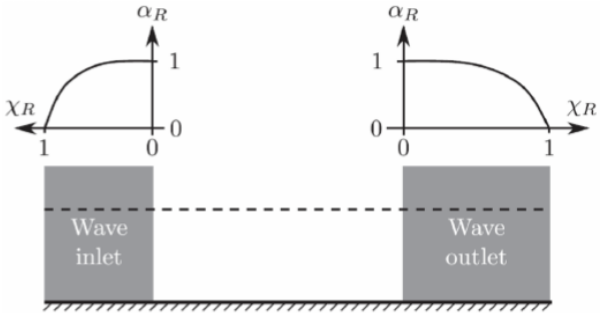

Fig. 1. Relaxation zone diagram for waves2Foam toolbox.

C. Dynamic mooring restraint model

For this study, MoorDyn is employed as the dynamic mooring solver, which is an open-source software widely used for analyzing floating offshore marine structures [15]. The solver is based on the lumped mass method, where the mooring line is discretized into small point masses, referred to as nodes. These nodes are interconnected using linear springs and dampers. At each node, line masses are combined with gravitational and buoyancy forces, hydrodynamic loads, and reactions from the seabed contact. The hydrodynamic drag and added mass are calculated using Morison's equation. The axial stiffness of the mooring line is represented by linear stiffness values assigned to each line segment, but only in tension. To mitigate nonphysical resonances arising from the lumped mass discretization, small internal damping can be added for each line segment. Bending and torsional stiffness are neglected in this model. The interaction with the seabed is simulated by incorporating vertical stiffness and damping forces when nodes pass below the seabed surface.

In this study, the latest version of MoorDyn, v2, is utilized. This new version provides enhanced capabilities for simulating floats and weights, allowing for a more comprehensive representation of the mooring system model required for the device under investigation.

III. SIMULATION CASES

D. Tank dimensions and wave conditions

Following the experimental procedure, the numerical wave tank (NWT) is utilized to generate and validate waves without the presence of the WEC system. The NWT is designed based on parametric dimensioning, tailored to the specific sea state by considering the wavelength (λ). In this study, a single sea state with significant wave height of $H_s = 0.2639$ m and peak wave period of $T_p = 2.16\ s$ (or $H_s = 7.39\ m$ and $T_p = 11.43\ s$ with 1:28 scaled ratio) is considered. It is noted that to provide consistent comparison with the experimental data. The results in Section 4 are displayed at full scale conditions.

The NWT is constructed with dimensions of 4.0λ in the wave propagation direction and 0.5λ in the transverse direction. The water depth is modelled to match the experimental setup, with a depth of 5.8 m. The still water level is set at 0 m, and the floating device is positioned 9 m downstream of the inlet. A wave probe is placed at 0.714 m upstream of the float's position for the benchmark of the generated wave heights. This position coincides with the reference wave probe specified in the experiment. A schematic of the tank setup is illustrated in Fig. 2.

To replicate the time series of the experimental wave heights, the irregular wave signal is transformed using Fast Fourier Transformation (FFT) into a combination of sinusoidal waves. The wave components including amplitudes, frequencies, and phases taken from the FFT serve as input for the numerical wave maker. A phase shift is also implemented in the wave component input to represent the non-zero location of the reference probe in the experiment. In the waves2Foam library, this input of wave components is facilitated using the 'irregular' wave options. For the signal decomposition, a total of 300

frequencies are employed to capture the characteristics of the wave signal.

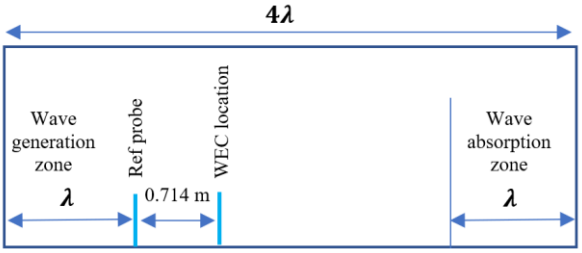

Fig. 2. Numerical wave tank schematic. The relaxation zones for wave generation and absorption are equal to one wave length, λ. The reference probe is placed at 0.714 m upstream of the WEC's location to be consistent with the experimental setup.

A mesh sensitivity study is also conducted to ensure the accuracy of the simulation results. In each mesh case, the computational domain is divided into multiple regions with varying mesh sizes. The smallest grid size is employed around the WEC system and the wave zone, while larger cells are utilized in regions further away from the wave zone and wave-fluid interaction area. The objective is to minimize the total number of grids while maintaining sufficient grid resolution around the areas of interest. The convergence analysis is performed using the following cell resolutions: 10, 15, 20, 25, and 30 cells per wave height (CPH). These values represent the grid sizes in the finest region of the mesh. Root-mean-square (RMS) values of the generated wave heights are compared with the finest grid to verify the convergence. Fig. 3 displays the constructed mesh for this study.

It is noted that in addition to simulating irregular wave signals, an equivalent regular wave case is also included in this study. Employing the assumption that the wave elevation follows a Rayleigh distribution, the maximum individual wave height during a sea state is calculated as $H_{max} = 1.9H_s$, and $T = T_p$. This equivalent regular wave case is simulated alongside the irregular wave conditions to assess the structural loads on the fixed device for comparative analysis. The objective is to determine whether the regular wave height, amplified by a factor of 1.9, can provide conservative results when compared to the irregular wave conditions. These findings will provide valuable insights into the potential use of the regular wave case for future studies, considering its significant reduction in computational time.

E. Experimental Validation Data

The experimental testing campaign was completed as part of the MARMOK-OWC project founded by DOE under FOA 2080 [14]. The main objective is advancing towards the commercial viability of IDOM's floating OWC technology by performing a detailed WEC design to fit PacWave-South site conditions. The physical model tests took place at the Offshore Technology Research Center (OTRC) in College Station, Texas, during July to September, 2021. The experiments were performed at a scale of 1:28.

F. Device geometry and free decay tests

The fundamental concept of the device involves a spar element that houses a cylindrical water column internally. An air chamber (orifice) is located at the upper section of the water column. The compression and decompression of this air chamber are channeled through self-rectifying air turbines. These turbines are connected to electric generators, which are controlled by power electronics. It is noted that due to the impossibility to scale down the turbine, a set of orifices are tested which introduce an equivalent damping to the water column than the turbine rotating at different rotational speeds. General dimensions of the device are provided in Fig. 4 and Table 1. As mentioned previously, to provide consistent comparison with the experimental data, results presented in Section 4 are scaled up and displayed at full scale values.

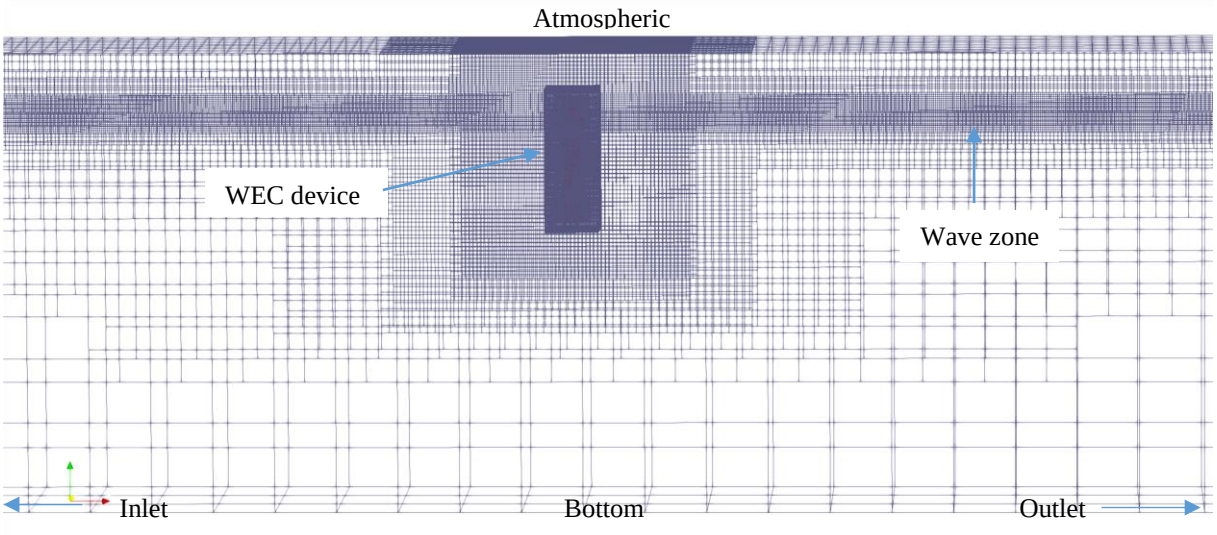

Fig. 3. Mesh construction for the numerical simulation. Finest resolution is used for the innermost region where the WEC system is placed, as well as the region at the wave elevation area. Outside these two zones, the grid is coarsening to reduce the computational resources.

Free decay tests are performed to quantify the motion of the device when subjected to an initial position offset, either in the heave or pitch degree of freedom. For this study, three free decay tests are carried out, two in heave (with and without the top orifice) and one in pitch (without the orifice).

From the free decay responses, two parameters consisting of the damped natural period and the damping coefficient are evaluated using a logarithmic decrement technique [20] to provide quantitative comparison with the experimental data. The following equations are employed for these calculations.

Damped natural period, T_d:

$$T_d = \frac{1}{n}\sum_{i=1}^{n} T_i \tag{8}$$

Damping coefficient or damping ratio (ζ):

$$\zeta = \frac{\delta}{\sqrt{4\pi^2 + \delta^2}} \tag{9}$$

With

$$\delta = \frac{1}{n}\ln\left(\frac{X_i}{X_{i+n}}\right) \tag{10}$$

Where T_i refers to the time it takes between successive peaks. The logarithmic decrement, δ, represents the rate at which the damped free response amplitude decays. Quantities X_i and X_{i+n} are peaks occurring n cycles apart beginning at the i^{th} oscillation cycle.

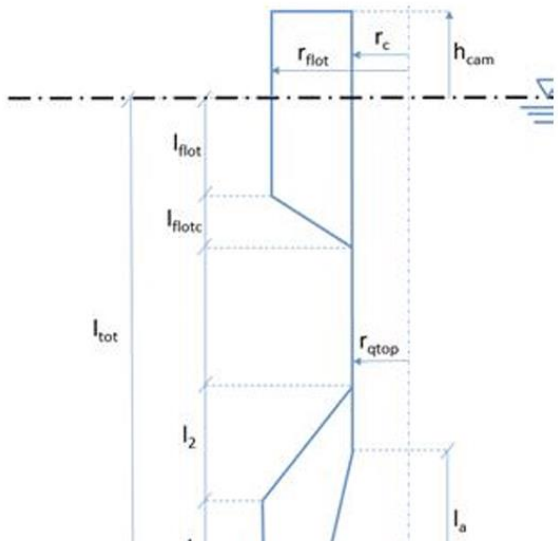

TABLE I
GENERAL DIMENSIONS OF THE MARMOK

Symbol	1:1 scale	1:28 scale
r_{flot} [m]	7.5	0.268
r_c [m]	3.75	0.134
l_3 [m]	8.0	0.286
l_{total} [m]	45.0	1.607
rq_{inf} [m]	7.5	0.268
h_{cam} [m]	6.5	0.232
Displacement [tonnes]	1948	0.089

For intellectual purposes, the results in this section will be normalized with the corresponding experimental outputs. It is also noted that although not presented in this paper, a mesh convergence study was also carried out in these tests to ensure numerical accuracy. The same grid resolutions from the wave generation cases were employed to carry out the simulations. These are chosen to satisfy the overset requirements that the background and the overset having similar resolutions. Final convergence for the damping ratio and damped natural period are 2.2% and 0.1%, respectively.

G. *Mooring system quasi-static benchmark*

Due to intellectual property reasons, a comprehensive description of the mooring configuration will not be provided in this paper, however a general overview is presented instead. The mooring system comprises four primary mooring lines that connect the four floats on the water surface to the seabed. These floats are interconnected by four Celda lines, while another set of four Conex lines links the floats to the WEC device. For a visual representation of the overall mooring system, please refer to Fig. 5.

Before performing the coupled floating simulations, the mooring configuration is benchmarked against experimental static test results. To carry out this section, the WEC body is displaced slowly/quasi-statically in the positive surge direction for 1.14 m (or 32 m full scale). The

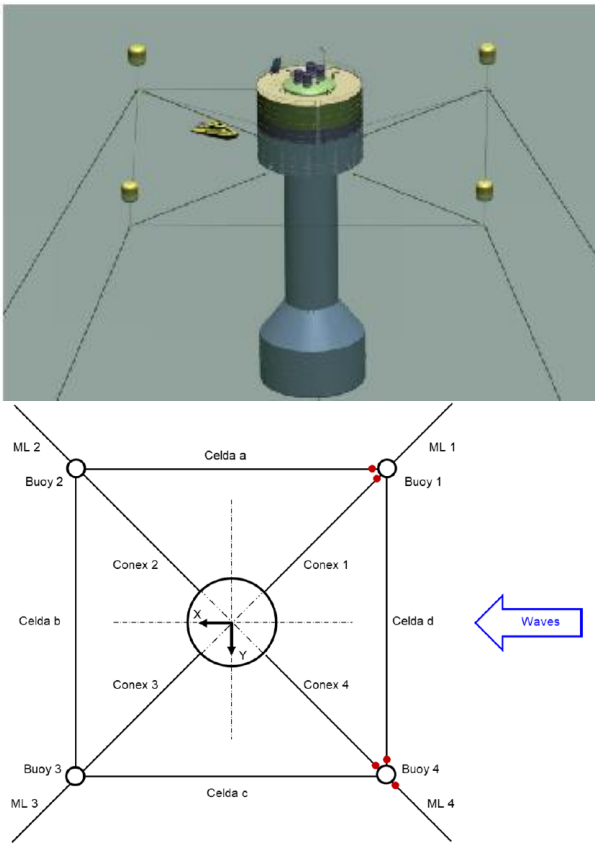

Fig. 5. Mooring system diagram [14]. The mooring system comprises four primary mooring lines that connect the seabed to four floats positioned on the water surface. These floats are interconnected by four Celda lines, while another set of four Conex lines links the floats to the WEC device.

pulling horizontal forces along with the lines' tensions on the main mooring line 4, the Celda D line, and the Conex 1 line are recorded (Fig. 5) simultaneously. The entire mooring system in this study is handled by MoorDyn including the dynamics and kinematics of the four floats.

H. *Fixed device subjected to extreme regular and irregular waves*

In this section, two simulations are performed where the WEC is stationary and subjected to extreme regular and irregular wave conditions as discussed in Section III.D. A 60-second period (~320 s at full scale) with high wave elevation is selected from the experimental wave signal out of a 3h duration extreme sea state (See Section I for the discussion of this high wave elevation period). It is noted that the results in this section are not directly compared to the experimental data due to the lack of measurements. They are, however, utilized to evaluate whether the regular wave condition, derived from the maximum wave components and amplified by a factor of 1.9, can yield conservative results compared to simulations using the full irregular wave condition.

The output parameters of this section include the structural loadings in the heave and surge directions, as well as the pressures along the body. The motions of the body are directly outputted as part of the sixDoFRigidBodyMotion solver. Additionally, 54 pressure probes are placed along the body, with 26 on each side, to measure the surface pressures. The pressure outputs are collected using the 'libforces' specified in the 'system/controlDict' of an OF case. The approximate locations of these pressure probes are illustrated in Fig. 6.

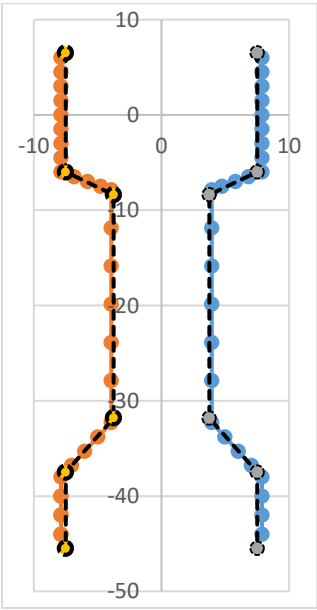

Fig. 6. Pressure probe locations on each side of the body. The dimensions shown are meters in full scale.

I. *Floating device subjected to extreme irregular waves*

This section focuses on the numerical model validation for the moored floating system under extreme conditions. To minimize uncertainties related to matching initial conditions, the simulation utilizes the first 60 s (~ 320 s at full scale) of data from the experimental measurements, rather than selecting a period with large wave heights as done in the previous section. The objective is to benchmark the responses of the WEC system, including motions in heave, surge, and pitch. Additionally, the mooring tensions on the main mooring line 4, and the Conex line 1 (Fig. 5) are also collected for comparison.

IV. RESULTS AND DISCUSSION

J. *Wave Generation*

Wave quality generated from different grid resolutions are displayed in Fig. 7 for comparison. The two snapshots depict the beginning of the wave signal and the period with the highest wave components. The Root Mean Square (RMS) values, calculated with respect to the finest mesh of 30 CPH, are 7.91%, 4.44%, 2.61%, and 1.61% for the mesh cases with 10, 15, 20, and 25 CPH, respectively.

Furthermore, the results from the 25 CPH grid are compared to the experimental wave signal in Fig. 7. Similarly, several snapshots of wave elevation collected from the reference wave probe are presented. Overall, the numerical wave model demonstrates good correlation with the experimental data. The maximum RMS value for the entire wave signal is estimated to be 6.1%, where the OpenFOAM wave elevations slightly deviate from the experimental heights, particularly around the wave crests and troughs. The differences could be attributed to the truncation of higher order terms of the wave signal when performing the FFT and its reconstruction input into

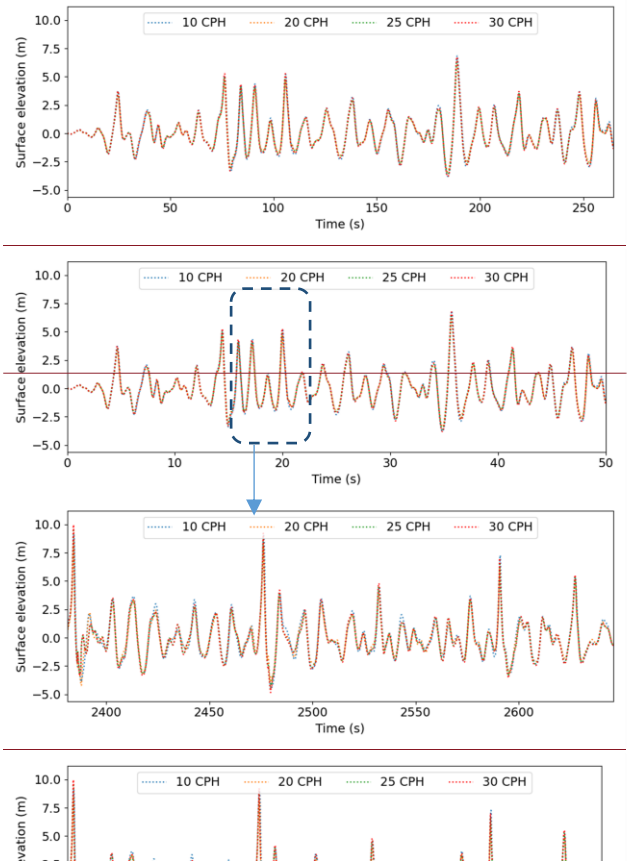

waves2Foam. Sensitivity tests could be examined further in future studies to improve the reconstruction of experimental irregular wave signal in the NWT. The overall results, however, are reasonable considering that a long wave signal (600s scaled and about an hour full scale) was successfully recreated with minimal wave reflection into the NWT.

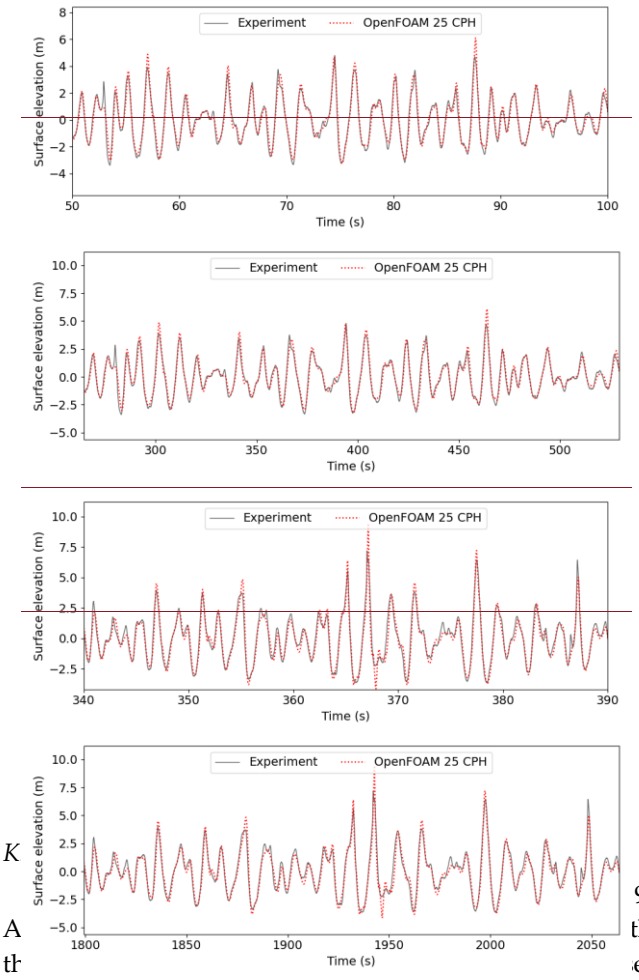

K 9. A th e.

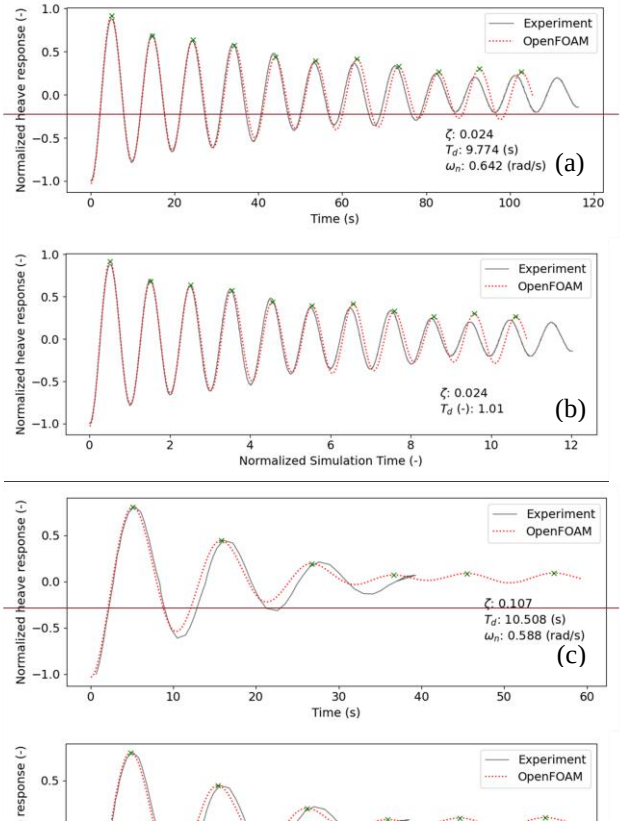

It can be observed that the heave responses for systems without the orifice closely match the experimental data, showing excellent agreement. However, the free decay in heave for the device with the orifice and the pitch response deviate from the experimental data. Table 2 provides a more quantitative comparison between the two datasets, presenting the mean values and associated uncertainties (standard deviation) obtained from the experiments.

As evident from Fig. 9, the heave decay test for the device without the orifice shows great correlation between the numerical predictions and the experimental results. The numerical values fall within the range (mean and uncertainties) recorded from the experimental tests. Conversely, for the heave decay test with the orifice, significant deviations can be observed, particularly in the damping coefficient compared to the experimental data. It is, however, worth noting that the associated uncertainty from experimental measurements for this parameter is substantial, reaching up to 11.73%. Additionally, the heave response exhibits high damping, resulting in only three cycles being recorded in the experiment compared to more than five cycles for the other cases. Since the damping coefficient and natural period are derived with a minimal number of cycles and given the high uncertainty values, these factors reasonably explain the differences between the two methods. Taking the uncertainty into account, the differences are reduced to within 7.5% and 6.5% for the damping coefficient and natural period, respectively.

TABLE II
FREE DECAY RESPONSE COMPARISON

		Experiment	OF	ε (%)
Heave (no orifice)	ζ (−)	0.0233 (0.0034)	0.024	3.00 (±14.59)
	T_d (s)	~~9.678~~1.000 (± 0.~~0210~~22)	~~9.774~~1.01	1.00 (± 0.22) ~~(0.22)~~
Heave (with orifice)	ζ (−)	0.0895 (0.0105)	0.107	19.55 (± 11.73)
	T_d (s)	~~11.462~~1.000 (±1.63)~~(0.18 71)~~	~~10.508~~ 0.917	8.32 (±1.63)~~(±1~~
Pitch (no orifice)	ζ (−)	0.0112 (0.0003)	0.012	7.14 (±0.27)
	T_d (s)	~~18.060~~1.000 (±0.08)~~(0.01~~	~~19.217~~ 1.064	6.41 (+0.08)

On the other hand, the numerically predicted pitch response is noticeably slower and less damped compared to the corresponding experiments. The pitch response is strongly influenced by the position of the center of gravity relative to the water line and the moment of inertia of the buoy. Acceptable measurement errors in these physical quantities can result in significant differences in pitch for models at the testing scale. It has been shown in [21] that even small uncertainties in center of gravity measurements can lead to substantial variations in pitch free decay

results. Furthermore, these variations could also be attributed to viscous effects. The turbulence model and the use of wall functions may underestimate the turbulent viscosity surrounding the body, thereby affecting the damping forces. Radiation damping in pitch is considerably smaller than in heave for this type of OWC, which explains why the viscous damping forces have a greater relative impact on the total damping in pitch compared to heave. This explains the better correlation of the results in heave compared to pitch.

L. *Mooring quasi-static tests*

The mooring force outputs from the static test are presented in Fig. 10, with corresponding experimental data plotted for comparison. The results indicate a good agreement between the two approaches in terms of mooring forces. Some minor deviations are observed specifically in the surge motion versus total pulling horizontal force. These deviations may be attributed to the uncertainty in the pulling trajectory of the system. In the OpenFOAM model, the pulling trajectory can be precisely controlled in the positive surge direction, whereas slight course deviations might occur during the experiments, leading to the observed differences. Nevertheless, these differences are minimal and do not appear to significantly impact the tensions in the mooring lines.

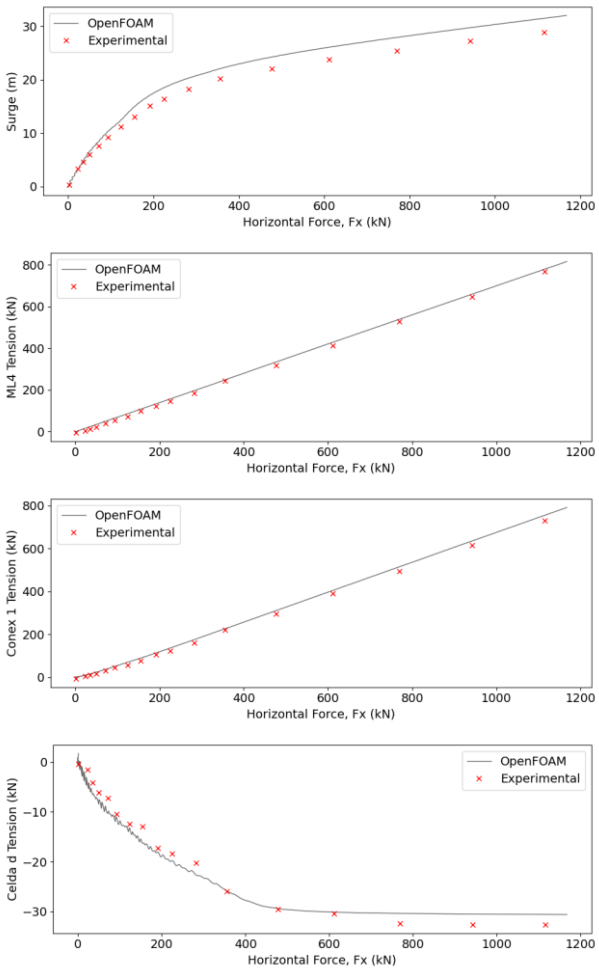

Fig. 10. Mooring tension results from quasi-static tests. For this test, the buoy is move quasi-statically in the positive surge direction while the total forces acting on the WEC and the mooring tensions are recorded.

M. *Fixed device in extreme regular and irregular waves*

The total loadings in surge and heave directions on the WEC body are presented in Fig. 11 subjected to both regular and irregular wave conditions, respectively. It is recalled that the regular wave conditions are simulated with $1.9H_S$ and the same wave period as the irregular wave case. On the other hand, maximum pressure outputs at each probe along the body are extracted from the simulations and plotted in Fig. 12. The probe numbers are ordered from top to bottom on the WEC with 26 probes on each side. The pressure values from the regular wave condition can be observed to consistently be higher than the irregular wave case. As expected, higher pressures are measured for probes at the WEC's bottom compared to the top surfaces. The results in this section demonstrated that structural loadings subjected to irregular wave conditions could be conservatively estimated employing the regular wave height and a multiplied factor of 1.9.

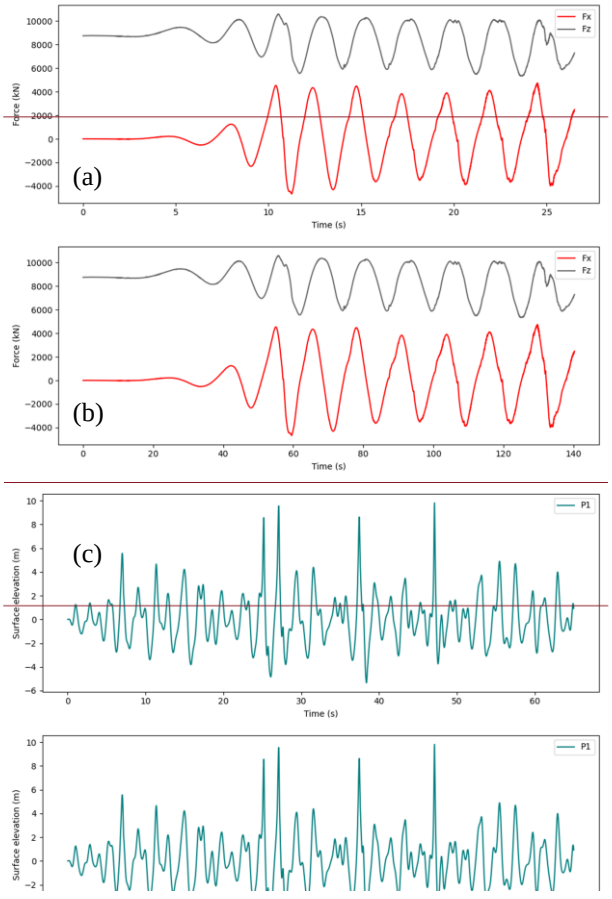

N. *Floating device subjected to extreme irregular waves*

Figs 13 and 14 display the motion responses of the WEC and the corresponding mooring tensions. In Fig 13, a strong correlation is observed between the heave and pitch motions in both the numerical model and experimental data. For the surge response, the numerical model and experimental data exhibit good agreement for the initial 60 seconds. Deviations, however, become noticeable between

60 and 120 seconds. During this period, while the WEC's position remains relatively constant in the simulation, it moves back towards the starting position in the

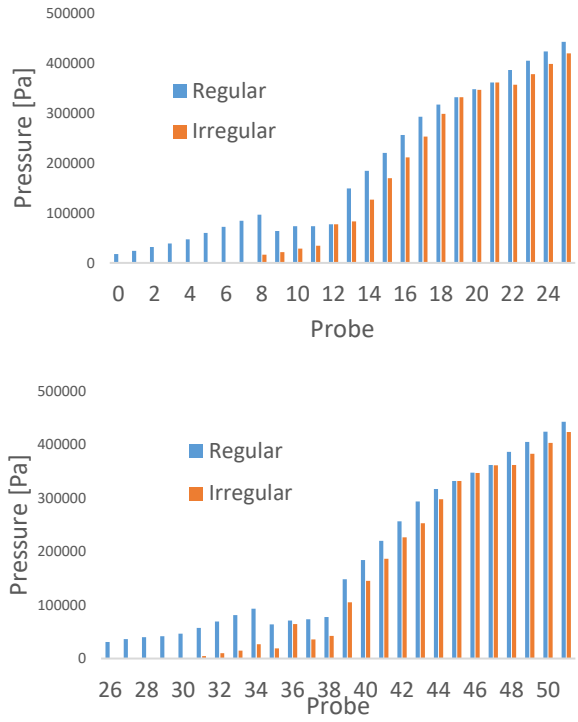

Fig. 12. Maximum pressure outputs from the body's surface are presented. 26 probes placed on each side of the body. The maximum pressures are extracted from the hydrodynamic loads as the device subjected to ~~each~~ regular and irregular

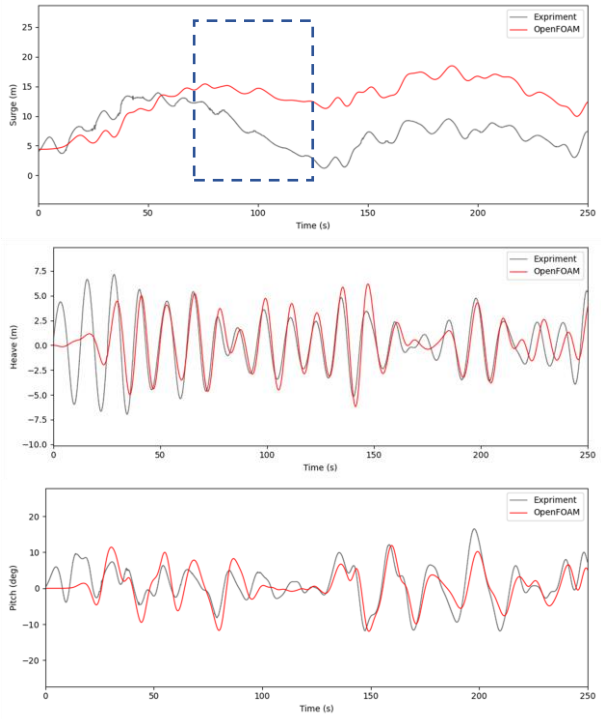

Fig. 13. Comparisons of the WEC's responses in Surge, Heave, and Pitch directions subjected to the first 250s of the irregular wave train between experimental and numerical methods. Heave and pitch results show very good correlation between the two datasets. Surge responses are also compared well except for the time marks from 60-120s (denoted by the dash box).

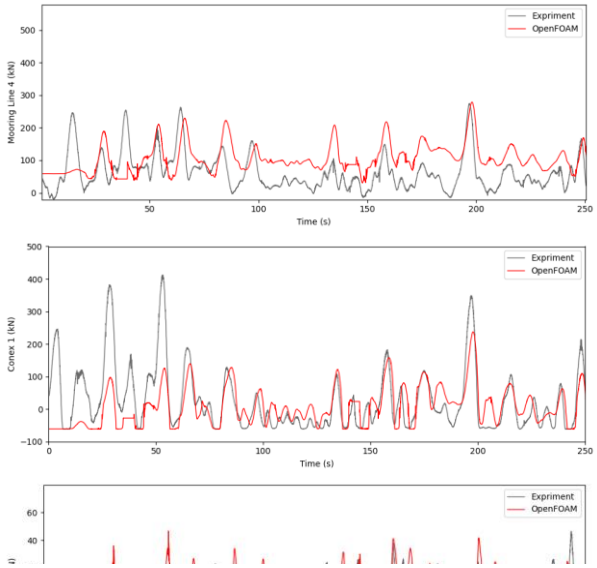

experiment. Correspondingly, the wave loads appear to be larger in the OF model compared to the laboratory forces. Beyond the 120-second mark, disregarding the shift resulting from the previous period, the trends in the two curves demonstrate great agreement. The reason for the deviation between 60 and 120 seconds is currently unknown and will be investigated in future analysis.

Figs 14 presents a comparison of the tensions in the main mooring line 4, and the Conex 1 line. The numerical output of Conex 1 exhibits good agreement with the experimental data, excluding the initial few cycles due to the ramping time. Regarding mooring line 4, the trend of the tension curve and its upper bound envelope closely correlate with the laboratory data. Starting from approximately 70 seconds, however, a shift in the magnitude of the simulation line's tensions compared to the measured data is observed. This shift can be attributed to the deviation of the WEC's surge position between 60 and 120 seconds.

V. CONCLUSION

In conclusion, the study addressed the research gap in numerical simulations of a floating WEC system under realistic extreme irregular waves, which are recreated with high accuracy from the laboratory signal. From the authors' knowledge, the study is also the first to present a quantitative comparison of the surface pressures and body's forces of the WEC system subjected to irregular wave and the equivalent regular wave conditions with $H_{max} = 1.9H_s$. This assumption has been employed in many studies but has not been quantitative and sufficiently demonstrated.

For the project, a high-fidelity CFD model for a 1:28 scale OWC-WEC MARMOK was developed and validated utilizing the overset mesh technique in the OpenFOAM package. waves2Foam and MoorDyn toolboxes were employed for wave generation, wave absorption, and mooring system modeling.

The laboratory extreme irregular wave inflow conditions were accurately reproduced. The numerical model was also validated against laboratory data obtained

from free decay tests consisting of heave (with and without the top orifice) and pitch (without top orifice) motions. While heave free decay without the orifice shows excellent agreement with experimental data, variations are noted for the heave with the orifice and pitch decay values. Factors influencing these derivations are discussed including high uncertainties of the experimental data, and high sensitivity of pitch motion relative to the center of gravity.

Structural loads on the device subjected to regular and irregular wave conditions were examined. Employing the factor of 1.9 for wave height, the loading and the pressure outputs along the body surface shows that the regular wave loads are conservatively, and adequately higher than the irregular condition values.

Simulation results of the floating WEC system, its motions, and the mooring loads were also presented. Heave and pitch behaviors follow closely with the experimental data while some deviations were noted for surge motion. Future study will explore this differences further. Correspondingly, the numerical output of the Conex 1 shows good agreement with the experimental data excluding the ramping time period. For mooring line 4, the trend of the tension curve and its upper bound envelop correlate well with the laboratory data.

Acknowledgement

This article has been authored by an employee of National Technology & Engineering Solutions of Sandia, LLC under Contract No. DE-NA0003525 with the U.S. Department of Energy (DOE). Funding was provided by the U.S. Department of Energy, Office of Energy Efficiency and Renewable Energy, Water Power Technologies Office under the Award Number DE-EE0008952. The employee owns all right, title and interest in and to the article and is solely responsible for its contents. The United States Government retains and the publisher, by accepting the article for publication, acknowledges that the United States Government retains a non-exclusive, paid-up, irrevocable, world-wide license to publish or reproduce the published form of this article or allow others to do so, for United States Government purposes. The DOE will provide public access to these results of federally sponsored research in accordance with the DOE Public Access Plan https://www.energy.gov/downloads/doe-public-access-plan.

References

[1] D. Ross, Power from the Waves. Oxford University Press, USA, 1995.

[2] M. Folley and T. J. T. Whittaker, “Analysis of the nearshore wave energy resource,” *Renewable Energy*, vol. 34, no. 7, pp. 1709–1715, Jul. 2009, doi: https://doi.org/10.1016/j.renene.2009.01.003.

[3] P. Malali and K. Marchand, “Assessment of currently available ocean wave energy conversion systems using technology readiness levels,” *International Journal of Renewable Energy Technology*, vol. 11, no. 2, p. 126, 2020, doi: https://doi.org/10.1504/ijret.2020.108332.

[4] V. S. Neary *et al.*, “METHODOLOGY FOR DESIGN AND ECONOMIC ANALYSIS OF MARINE ENERGY CONVERSION (MEC) TECHNOLOGIES.,” *www.osti.gov*, Apr. 01, 2014. https://www.osti.gov/servlets/purl/1143279.

[5] R. G. Coe *et al.*, “CFD design-load analysis of a two-body wave energy converter,” *Journal of Ocean Engineering and Marine Energy*, vol. 5, no. 2, pp. 99–117, May 2019, doi: https://doi.org/10.1007/s40722-019-00129-8.

[6] E. Katsidoniotaki *et al.*, “Validation of a CFD model for wave energy system dynamics in extreme waves,” *Ocean Engineering*, vol. 268, p. 113320, 2023. doi:10.1016/j.oceaneng.2022.113320

[7] Jennifer Van Rij, Yi Hsiang Yu, and T. Tran, “Validation of simulated wave energy converter responses to focused waves,” *Proceedings of the Institution of Civil Engineers - Engineering and Computational Mechanics*, vol. 174, no. 1, pp. 32–45, Mar. 2021, doi: https://doi.org/10.1680/jencm.19.00039.

[8] C. Windt *et al.*, “Validation of a CFD-based numerical wave tank model for the power production assessment of the wavestar ocean wave energy converter,” *Fluids*, vol. 146, no. Wind and Wave Renewable Energy Systems, pp. 2499–2516, Feb. 2020, doi: https://doi.org/10.1016/j.renene.2019.08.059.

[9] C. Windt *et al.*, “Validation of a CFD-Based Numerical Wave Tank Model of the 1/20th Scale Wavestar Wave Energy Converter,” *Fluids*, vol. 5, no. 3, p. 112, Jul. 2020, doi: https://doi.org/10.3390/fluids5030112.

[10] E. J. Ransley, D. M. Greaves, A. Raby, D. Simmonds, M. M. Jakobsen, and M. Kramer, “RANS-VOF modelling of the Wavestar point absorber,” *Renewable Energy*, vol. 109, pp. 49–65, Aug. 2017, doi: https://doi.org/10.1016/j.renene.2017.02.079.

[11] E. Katsidoniotaki and M. Göteman, “Numerical modeling of extreme wave interaction with point-absorber using OpenFOAM,” *Ocean Engineering*, vol. 245, p. 110268, Feb. 2022, doi: https://doi.org/10.1016/j.oceaneng.2021.110268.

[12] E. Katsidoniotaki, E. Nilsson, A. Rutgersson, Jens Engström, and Malin Göteman, “Response of Point-Absorbing Wave Energy Conversion System in 50-Years Return Period Extreme Focused Waves,” *Journal of Marine Science and Engineering*, vol. 9, no. 3, pp. 345–345, Mar. 2021, doi: https://doi.org/10.3390/jmse9030345.

[13] L. Sjökvist, J. Wu, E. Ransley, J. Engström, M. Eriksson, and M. Göteman, “Numerical models for the motion and forces of point-absorbing wave energy converters in extreme waves,” *Ocean Engineering*, vol. 145, pp. 1–14, Nov. 2017, doi: https://doi.org/10.1016/j.oceaneng.2017.08.061.

[14] de M. Para and Borja, “MARMOK-OWC project; Final Technical Report,” *www.osti.gov*, Oct. 10, 2022. https://www.osti.gov/biblio/1907549 (accessed May 30, 2023).

[15] M. Hall, “MoorDyn V2: New Capabilities in Mooring System Components and Load Cases,” Dec. 2020, doi: https://doi.org/10.1115/omae2020-19341.

[16] N. G. Jacobsen, D. R. Fuhrman, and J. Fredsøe, “A wave generation toolbox for the open-source CFD library: OpenFoam®,” *International Journal for Numerical Methods in Fluids*, vol. 70, no. 9, pp. 1073–1088, Nov. 2011, doi: https://doi.org/10.1002/fld.2726.

[17] H. Weller, "Derivation, modelling and solution of the conditionally averaged two-phase flow equations. Nabla Ltd." *No Technical Report TR/HGW* 2. *Nabla Ltd* 2, 2002.

[18] H. Rusche, “Computational fluid dynamics of dispersed two-phase flows at high phase fractions,” Imperial College London (University of London), 2003.

[19] G. Joel, “Overset Composite Grids for the Simulation of Complex Moving Geometries,” pp. 1–1, Jan. 2006.

[20] D. J. Inman, Engineering Vibration. 2001.

[21] J. Palm, C. Eskilsson, G. M. Paredes, and L. Bergdahl, “Coupled mooring analysis for floating wave energy converters using CFD: Formulation and validation,” *International Journal of Marine Energy*, vol. 16, pp. 83–99, Dec. 2016, doi: https://doi.org/10.1016/j.ijome.2016.05.003.